Carbohydrate Polymers 289 (2022) 119455

Contents lists available at ScienceDirect

Carbohydrate Polymers

journal homepage: www.elsevier.com/locate/carbpol

Pheophorbide A and SN38 conjugated hyaluronan nanoparticles for photodynamic- and cascadic chemotherapy of cancer stem-like ovarian cancer

Junghan Lee [a,b], Enkhzaya Davaa [a], Yixin Jiang [a,b], Kyung-Ju Shin [a], Min Hye Kim [d], Hyunsu An [c], Jinho Kim [d], Steve K. Cho [c], Su-Geun Yang [a,b,*]

[a] Department of Biomedical Science, BK21 FOUR Program in Biomedical Science and Engineering, Inha University College of Medicine, Incheon 22212, Republic of Korea
[b] Inha Institute of Aerospace Medicine, Inha University College of Medicine, Incheon 22332, Republic of Korea
[c] School of Life Sciences, Gwangju Institute of Science and Technology (GIST), Gwangju 61005, Republic of Korea
[d] Department of Chemistry, Research Institute of Basic Sciences, Incheon National University, Incheon 22012, Republic of Korea

ARTICLE INFO

Keywords:
Hyaluronan-cholesterol conjugate
Combination chemotherapy
Cancer stem cell (CSC) makers
Photodynamic therapy
SN38
Hyaluronan nanoparticles
Chemo-resistant ovarian cancer
Thioketal drug conjugate
CD44-targeting

ABSTRACT

In this study, we designed photo-triggered reactive oxygen species (ROS)-generating pheophorbide A and ROS-cleavable thioketal-SN38 conjugated hyaluronan-cholesterol nanoparticles (PheoA-SN38-HC NPs). And we observed the combined therapeutic effects of PheoA-SN38-HC NPs against HEY-T30 human ovarian cancer (OC) model. Clinical Proteomic Tumor Analysis Consortium (CPTAC) data showed that the expression of cancer stem cell (CSC) markers (CD44, ALDH1A1, and CD117) is highly associated with poor clinical outcomes in OC patients. We proved that HEY-T30 cells overexpress CSC markers and much more invasive than other cancer cells. Flow cytometry (FACS) and microscopic analysis revealed the active targeting property of PheoA-SN38-HC NPs to CD44+ HEY-T30 cells. Moreover, the combination therapeutic effect of PheoA-SN38-HC NPs was clearly demonstrated against in vitro HEY-T30 cells and an in vivo xenograft mouse model. In particular, the paracrine cytotoxic effect of SN38 probably compensates the locoregional therapeutic limitation of photodynamic therapy.

1. Introduction

Ovarian cancer (OC) is the seventh most common cancer and the eighth leading cause of cancer-related death (Torre et al., 2018). The American Cancer Society (ACS) expects that about 22,530 new cases of ovarian cancer will be diagnosed in 2020. The ACS also reports that 13,980 people die from ovarian cancer in the United States throughout the year. Recently, understanding of molecular targets and tumor microenvironment has facilitated the advent of new target drugs for OC treatment. However, OC is still a major cancer with a high mortality rate (Carioli et al., 2019). There is a desperate need to optimize the currently available treatments and develop new therapeutic strategies.

SN38 (7-ethyl-10-hydroxycamptothecin), a bio-active metabolite of irinotecan (CPT-11, water-soluble drug of the alkaloid camptothecin), is an inhibitor of topoisomerase I, a key nuclear enzyme involved in DNA double helix supercoiling during cell replication, and has high anti-proliferative efficacy for many kind of tumors including ovarian cancer, mammary cancer, colon cancer and lung cancer (Zhang et al., 2004). Especially, SN38 is a thousand times more toxic than irinotecan itself (Xie et al., 2002; Perrone et al., 2020; Tahara et al., 2014). However, SN38 could not be directly applied to clinical therapy of cancer because of its poor solubility (Santi et al., 2014). Up to now, to improve its water solubility and bioavailability, numerous studies related to drug delivery systems such as PEG conjugation, polymer micelle, and liposome formulation are ongoing (Sadzuka et al., 2005; Miyazaki et al., 2014; Govindan et al., 2013).

Conventional chemotherapy is the most common choice for majority of ovarian cancer. However, subpopulations of cancer cells, now defined as cancer stem cells (CSC), acquire drug-resistance and induce tumor recurrence and metastasis (Ayob & Ramasamy, 2018; Najafi et al., 2019). CSC targeting therapy can improve the therapeutic efficacy of conventional chemotherapy. However, universal markers for CSC target therapy have not been clearly identified. CSCs are composed of multiple heterogeneous cells. The heterogeneity of CSCs is the major challenge in

* Corresponding author at: Department of Biomedical Science, Inha University College of Medicine, B-308, Chungsuk Bldg, 366, Seohae-Daero, Jung-Gu, Incheon 22332, Republic of Korea.
E-mail address: sugeun.yang@inha.ac.kr (S.-G. Yang).

https://doi.org/10.1016/j.carbpol.2022.119455
Received 23 October 2021; Received in revised form 24 March 2022; Accepted 31 March 2022
Available online 7 April 2022

discovering universal markers (Shibata & Hoque, 2019). Therefore, there is an urgent need to discover and identify novel CSC markers for more effective cancer treatment.

Combination therapy, if combined together with CSC targeting functions and other therapeutic regimens, can be an another breakthrough approach to overcome the clinical dilemmas mentioned above (Arbour & Riely, 2019; Lee et al., 2019). Photodynamic therapy (PDT) is a good therapeutic modality for combination treatment of both CSCs and non-CSC tumor cells (Holohan et al., 2013; Lee et al., 2019; Longley & Johnston, 2005; Riganti & Contino, 2019; Swanton, 2012). Reactive oxygen species (ROS) generated by photosensitizers under laser treatment are cytotoxic enough to induce apoptosis of total tumor cells. Furthermore, PDT does not cause the serious side effects that plague in radio- and chemotherapy (Gottesman, 2002; Li et al., 2008; Park et al., 2000; Park et al., 2008).

We hypothesize that combination design of CSC marker-specific targeting with PDT and chemo-agents will be more effective for treating chemo-resistant cancers which may overexpress cancer stem cell markers. We introduce a photosensitizer, pheophorbide A (PheoA), and chemodrug, SN38 (7-ethyl-10-hydroxycamptothecin, DNA topoisomerase I inhibitor), using ROS-cleavable linkers into CD44 (as one of typical CSC markers) targeting hyaluronan (HN) nanoparticles (Scheme 1). Until now, HN-based nanomedicine and conjugation design have been extensively studied (Angeles & Nesporova, 2021; Wang et al., 2021; Zhang et al., 2020). ROS-triggered drug release provides an attractive means of achieving synergistic concomitant chemotherapy with PDT. Thioethers, di-selenium linker, thioketals, boronic acid esters, and aminoacrylates are ROS-cleavable linkers that release linked chemo agents by cancer cell-specific ROS (Kim et al., 2016; Xiao et al., 2015; Yu et al., 2011). The therapeutic feasibility of combination-designed HN nanoparticles was evaluated against HEY-T30 human ovarian cancer cells. Chemo-resistance of HEY-T30 cells have been widely studied (Brouwer-Visser et al., 2014a; Huang et al., 2010), and we evaluated the expression of CSC markers in HEY-T30 cells in western blot assay and its invasiveness in migration and colony forming assay. Moreover, in accordance with CSC markers in HEY-T30 cells, clinical relevance of CSC markers (CD44, ALDH1A1, and CD117) in OC was analyzed using proteomics data of human ovarian cancers provided from The Clinical Proteomic Tumor Analysis Consortium (CPTAC) (Rudnick et al., 2016). For the proof of synergistic effects of combination design, we visualized the CD44-specific targeting efficacy, PDT plus SN38 combination effect, and paracrine cytotoxic effect of SN38 to off-PDT region with in vitro and in vivo HEY-T30 xenograft BALB/c nude mouse model.

2. Experimental section/methods

2.1. Materials

Sodium hyaluronate (Mw 21,000–40,000) was purchased from Lifecore Biomedical (MN, USA). Pheophorbide A was obtained from Frontier Scientific, Inc. (UT, USA). SN38 (7-ethyl-10-hydroxycamptothecin) was provided by Xian Yiyang Bio-Tech (Shaanxi, China). Cholesteryl chloroformate, ethylenediamine, hexamethylenediamine, cysteamine, ethyltrifluoroacetate, p-toluenesulfonic acid monohydrate, 2-methoxypropene, and 1-ethyl-3-(3-dimethylaminopropyl)carbodiimide (EDC) were purchased from Sigma. All solvents were of HPLC grade and purchased from Duksan Chemicals Co. (Gyeonggi-do, Korea).

2.2. Analysis of CPTAC proteomics data of ovarian cancer tissues

Proteomics data of ovarian tumors provided from The Clinical Proteomic Tumor Analysis Consortium (CPTAC) were analyzed. A subset of The Cancer Genome Atlas Ovarian Cancer samples (122 tumor samples) was characterized by mass spectrometry-based proteomics using CPTAC (Zhang et al., 2016). The processed proteomics data (normalized log2-transformed relative protein amount) of the CPTAC study 'TCGA Ovarian Cancer' was downloaded via Aspera Connect program and further processed in Python. Further analysis was performed as previously described (Longley & Johnston, 2005). Odds ratios (ORs) with 95% confidence interval (CI) were employed to evaluate the association between expression of CD44 and ALDH1A1 and the response to therapy (complete remission or poor outcome) for patients with ovarian cancer.

Next, the impact of genetic alterations of CSC markers on the survival of patients with ovarian cancer was analyzed (Gao et al., 2013). A survival plot was drawn on cBioPortal using CD44, CD177, and ALDH1 as inputs. Patients were divided into two groups based on the genetic alteration status of CD44, CD177, and ALDH1, and differences in

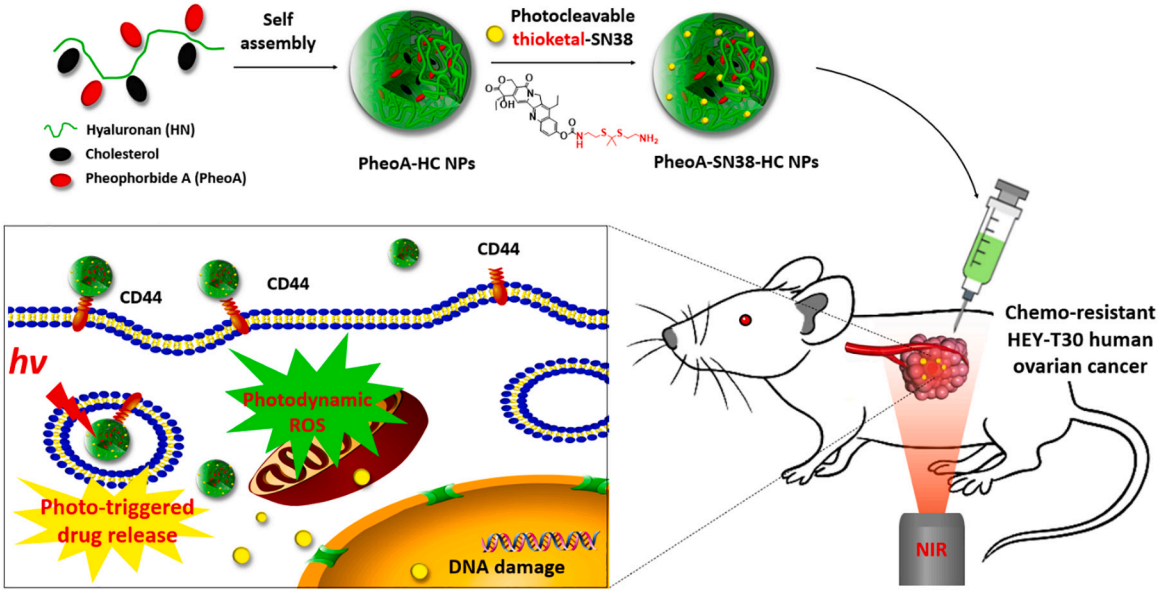

Scheme 1. Photodynamic ROS-generating PheoA and ROS-trigger SN38 releasing combination-therapeutic hyaluronan nanoparticles (PheoA-SN38-HC NPs), designed to overcome ovarian cancer therapy, demonstrated a combined therapeutic efficacy on growth inhibition of HEY-T30 ovarian cancer in xenograft mouse models. HEY-T30 human ovarian cancer cells show high expression of cancer stem cell (CSC) makers (CD44, ALDH1A1 and CD117).

survival rates were analyzed.

2.3. Expression of CSC markers in chemo-resistant cancer cells

2.3.1. Chemo-resistant cancer cells and cell culture

Paclitaxel resistant HEY-T30 human ovarian cancer cells (CRL-3252™, American Type Culture Collection, VA) were selected for this study. HCT 116 cells, RKO cells (human colon cancer cells), and HEK 293 cells (human embryonic kidney cell) were included in the study to estimate expression of CSC markers (Debeb et al., 2010; Kondo, 2007; Szarynska et al., 2017). Cells were cultured in DMEM (Dulbecco's Modified Eagle Medium) with 10% FBS (fetal bovine serum) and 1% penicillin/streptomycin (PS). Other cells were grown in RPMI 1640 (Roswell Park Memorial Institute Medium) with 10% FBS and 1% PS.

2.3.2. Colony formation assay

Cells (500 cells/well) were seeded into 6-well plates. After further incubation for 8 days at 37 °C, cells were fixed with 4% formalin and stained with 2% crystal violet for 10 min.

2.3.3. 2D migration assay

Cells were seeded into a block and scratcher (SPL; 2 block wells) at a density of 1×10^6 /well in serum-free medium. After incubation at 37 °C in 5% CO_2 for 12 h, a wound was formed by the scratcher and washed with fresh medium. Cell migration was detected with microscopy at 0 and 24 h.

2.3.4. Western blot assay of CSC markers

Expression of CD44, CD117, and ALDH1A1 in HEY-T30, HEK 293, HCT 116, and RKO cells was assessed using western blots. Cells were lysed in buffer RIPA (0.1% SDS, 0.5% sodium deoxycholate, 1% Nonidet P-40, 150 mM NaCl, 50 mM Tris-HCl pH 8.0) and a cocktail of protease inhibitors (1 mM phenylmethylsulfonyl fluoride, 2 μg/ml aprotinin, and 2 μg/ml leupeptin). Equal amounts of proteins (40–60 μg) were individually run on 15% SDS-PAGE and 10% SDS-PAGE, transferred in the PVDF (polyvinylidene difluoride) membrane (Millipore, Bedford, MA), blocked in 3% (w/v) non-fat milk, and incubated with different primary antibodies at 4 °C overnight. Primary antibody sources were CD44 (37259s; Cell Signaling Technology), CD117 (3074s; Cell Signaling Technology), and ALDH1A1 (12035; Cell Signaling Technology).

After washing with TBST (0.1% Tween 20 included tris-buffered saline) buffer three times, membranes were incubated with HRP-conjugated goat anti-rabbit or anti-mouse secondary antibodies (Santa Cruz Biotechnology, Dallas, TX) at room temperature for 2 h. The protein bands were obtained by a gel image analyzer.

2.4. Preparation of HN nanocarrier with combination therapeutic design

2.4.1. Introduction of photodynamic ROS-generating pheophorbide A

First, cholesterol, a hydrophobic core-forming moiety, was introduced to HN as previously described (refer to Supporting information) (Byeon et al., 2018). The acquired HN-cholesterol polymer spontaneously formed spherical nanoparticles (HN-cholesterol nanoparticles; HC NPs) in water phase as shown in our previous study (Lee et al., 2016). Then, HC polymer was further introduced to a reaction with pheophorbide A (PheoA) to acquire photodynamic NPs (PheoA-HC NPs). Briefly, PheoA (10 mg) was conjugated with 200 μl of ethylenediamine in the presence of EDC (50 mg) and 4-dimethylaminopyridine (DMAP, 10 mg) in 10 ml of dichloromethane for 24 h at room temperature. Aminated PheoA was purified using a desalting column (Sephadex G-10) and freeze dried. HC polymers (20 mg) were then reacted with 3 mg of PheoA-amine (m.w. = 634.77) in DMSO solution after mixing with 10 mg of EDC, and PheoA-HC polymer was purified by dialysis membrane with 100 K MWCO.

2.4.2. Introduction of ROS-cleavable SN38

PheoA-HC was conjugated with ROS-cleavable SN38 (compound **4**, Fig. S1). ROS-cleavable thioketal linker and SN38 conjugates were synthesized as shown in Supporting information Fig. S1. Briefly, 10 mg of PheoA-HC was conjugated with 12.3 mg of compound **4** (Fig. S1) in the presence of 38 mg of EDC in DMSO overnight. The acquired polymer (PheoA-SN38-HC) was purified by dialysis and dissolved in water. For the control study, non-cleavable SN38 was introduced to another PheoA-HC using compound **5**.

2.5. Characterization of PheoA-SN38-HC NPs

The synthesized PheoA-SN38-HC was analyzed by magnetic resonance spectroscopy (Avance III 400 MHz, Bruker, MA, USA). Particle size and morphology were measured using transmission electron microscopy (JEOL JEM-1011, JEOL, Tokyo, Japan) and dynamic light scattering (Zetasizer Nano ZS90, Malvern, UK).

2.6. In vitro evaluation of NIR-responsive ROS generation and ROS-triggered SN38 release

2.6.1. Estimation of NIR-responsive ROS generation

To evaluate generation of singlet oxygen species, PheoA-SN38-HC NPs were exposed to NIR light and subjected to DMA (9, 10-dimethylanthracene) testing (Gomes et al., 2005). DMA (final conc. 100 μM) in DMSO was added to HC, PheoA-HC, or PheoA-SN38-HC NPs (1 mg/ml), and samples were directly exposed to NIR laser ($\lambda = 671$ nm, 167 mW/cm^2, Shanghai Laser & Optics Century Co., Ltd., China) for 0, 1, 2, 3, 4, 5, 10, and 30 min. Fluorescence intensities at $\lambda_{max} = 420$ nm of DMA were measured using a microplate reader (Infinite 200 pro, Tecan, Wine, Austria). Simultaneously, cellular disposition of singlet oxygen generated from PheoA-SN38-HC NPs under NIR irradiation was assessed. NPs, SOSG, and ethidium homodimer-1 (Invitrogen, CA) were added to cells, followed by irradiation with NIR for 10 min ($\lambda = 671$ nm, power = 167 mW/cm^2). Cells were then incubated for 2 h, fixed with PFA, and introduced to a fluorescence microscope.

2.6.2. Estimation of ROS-triggered release of SN38

The amount of SN38 released from PheoA-SN38-HC NPs under NIR irradiation was measured by analyzing fluorescence spectra of free SN38. Briefly, two types of HC-PheoA-SN38 NPs conjugated with photocleavable SN38 or non-cleavable SN38 were respectively dissolved in DMSO at the concentration of 1 mg/ml, exposed to NIR for different times, and precipitated by ultracentrifugation at 400,000 rpm for 30 min. Supernatants containing SN38 released from NPs were collected, and fluorescence spectra were obtained using a microplate reader (excitation 360 nm/emission 400–600 nm). The amount of SN38 released from NPs was calculated using a pre-established standard calibration curve of SN38 solutions (0–50 μg/ml).

2.7. In vitro cell studies for functional assay of combination design

2.7.1. CD44-CSC marker specific cellular uptake of NPs

Cells were cultured on 8-well chambered coverslips for uptake studies. 50 μg/ml of NPs (PheoA-HC NPs or PheoA-SN38-HC NPs) were added to CD44$^+$ HEY-T30 cells (5×10^4 cells, 500 μl medium) with or without HN (100 μg/ml), incubated for 4 h, fixed with 4% paraformaldehyde, and stained with DAPI. Cells were examined under a confocal microscope (FV1000, Olympus, Japan) and a fluorescence microscope (CELENA® S, Logos Biosystems, South Korea).

2.7.2. Estimation of cytotoxicity of NPs based on combination design

A water-soluble tetrazolium (WST) assay was performed to determine the cellular toxicity of NPs. Briefly, HEY-T30 cells (4×10^4/well) were seeded on a 96-well plate and cultured in a 5% CO_2 incubator at 37 °C overnight. To evaluate toxicities, HC NPs, PheoA-HC NPs, or HC-

PheoA-SN38 NPs at final concentrations of 0, 5, 10, 20, or 50 μg/ml were added to wells; 24 h later, WST-1 reagent was added. Cell viabilities were determined by measuring absorption values at 450 nm. Under the same procedure, synergistic cytotoxic effects of combination treatment (photodynamic PheoA and chemotherapeutic SN38) were evaluated using HC-PheoA-SN38 NPs.

2.7.3. Paracrine cytotoxic effect of ROS-trigger released SN38

To examine trigger-released SN38 release and its paracrine effect, HEY-T30 cells were incubated on 8-well chambered coverslips with PheoA-HC NPs or HC-PhoeA-SN38 NPs for 4 h. Then, HEY-T30 cells in the left side of the well were irradiated using 670 nm NIR (100 J/cm^2). At 24 h post-irradiation, cells were co-stained with Calcein AM (live cells, green) and ethidium homodimer-1 (dead cells, red) according to the manufacturer's protocol (Invitrogen, CA, USA). After washing with fresh PBS buffer 3 times, cells were fixed with 4% PFA (paraformaldehyde) and analyzed by fluorescence microscopy and confocal microscopy.

2.8. In vivo tumor targeting study

All animal experiments were performed at the Animal Research Laboratory at Inha University and approved by the Inha University's Animal Care Committee (IUACC, INHA 201030-732). HEY-T30 cells (2 × 10^6) were subcutaneously injected into the backs of BALB/c nude mice. After two weeks, mice were divided into four groups ($n = 3$) and PBS, Cy5-HC NPs (1 mg/kg) with or without HN (1 mg/kg) were injected into tail vein. In the case of HN + Cy5-HC NPs treated groups, HN was pre-injected 30 min before Cy5-HC NPs treatment. After 72 h, each mouse images were obtained by in vivo image analyzer (FOBI, NEO science, South Korea). Then, the organs (heart, lung, spleen, liver, kidney, and tumor) were harvested, and fluorescence intensity of each organ was analyzed by ImageJ software. After sectioning of tumors with 50 μm thickness by cryotome, tumor slices were further stained with DAPI and obtained their fluorescence images by confocal microscope.

2.9. In vivo tumor growth inhibition study

HEY-T30 cells (2 × 10^6) were subcutaneously injected into the backs

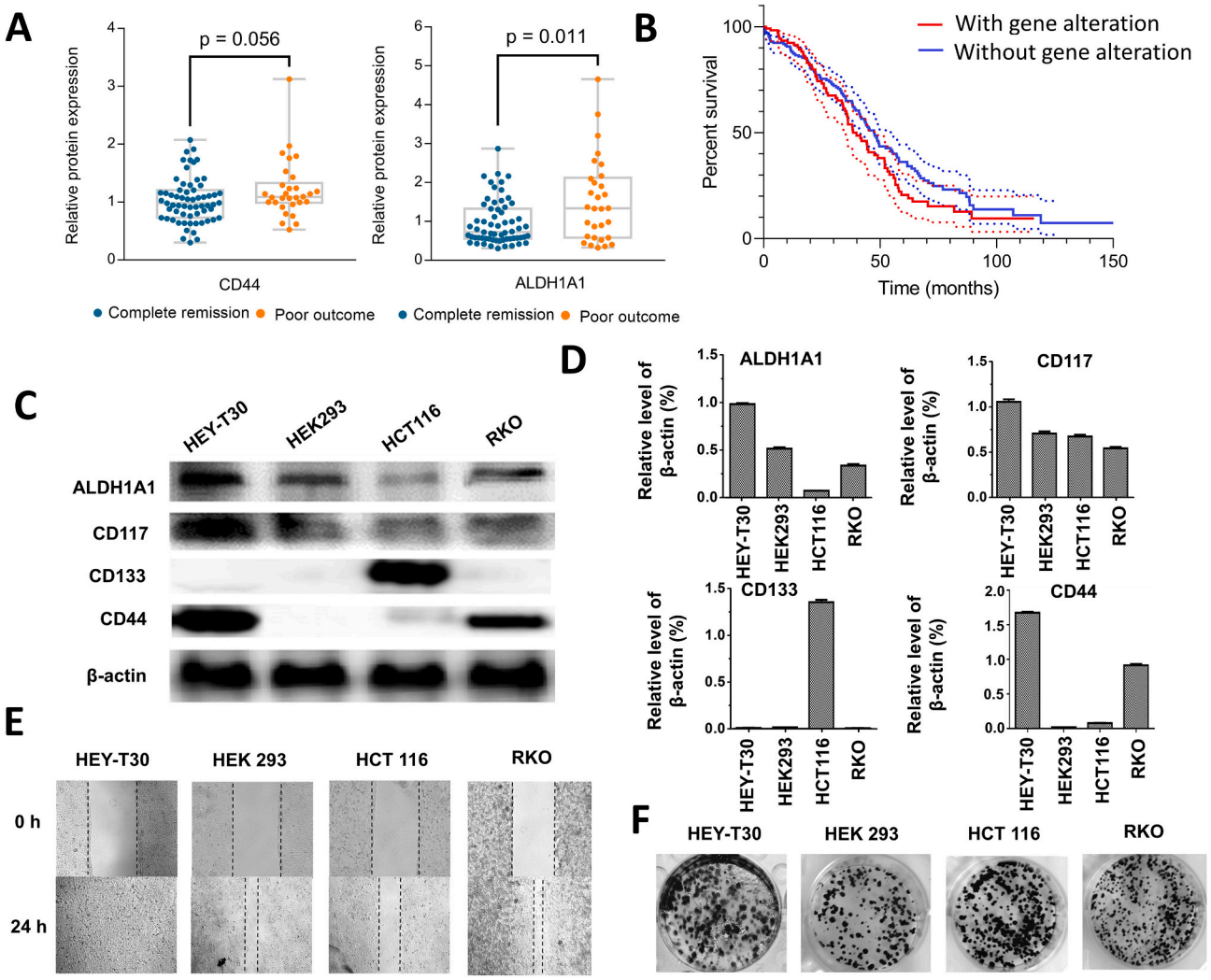

Fig. 1. Clinical relevance of CSC markers in ovarian cancer patient CPTAC proteomics data, and HEY-T30 human ovarian cancer cells with high expression of CSC markers. A. Analysis of CPTAC proteomics data of ovarian cancer patient tissues. CPTAC proteomics data support relationship between expression of two CSC markers (CD44 and ALDH1A1) and ovarian cancer (OC) progression. B. Impact of CSC markers genetic alteration (*CD44*, *CD177*, and *ALDH1* genes) on survival of ovarian cancer patients. C and D. Expression of CSC markers (ALDH1A1, CD117, CD133 and CD44) by western blot in HEY-T30 ovarian cancer cells, HCT116 and RKO colon cancer cells, and HEK 293 human embryonic kidney cells. HEY-T30 cells, showed the strongest ALDH1A1, CD44 and CD44 expression. E. 2D cell migration assays of four pairs of cell lines. F. Colony formation assay proved HEY-T30 cells show the strongest colony forming power. Yanqing et al. reported that CD44 is the most powerful controlling factor for ovarian cancer cell invasion, migration, and colony formation.

of BALB/c nude mice. When primary tumors reached ~100 mm^3, mice were divided into four groups ($n = 5$) and PBS, HC NPs, HC-PhoeA NPs, or PheoA-SN38-HC NPs were injected into tumors at a dose of 10 mg/kg. Each tumor region was irradiated with NIR (λ = 671 nm, 100 J/cm^2) once a day for three consecutive days. Tumor sizes and body weights were measured daily. Mice were sacrificed 4 weeks after injection of NPs, and tumors were recovered. Excised tumors were analyzed by hematoxylin and eosin (H&E) staining and terminal deoxynucleotidyl transferase dUTP nick end labeling (TUNEL) assay.

3. Results

3.1. CSC markers in human OC tissues and clinical implications

3.1.1. CPTAC proteome data and CSC markers in OC tissues

As shown in Fig. 1A, our analysis of CPTAC proteome data of TCGA ovarian cancer tumor samples suggested that high expression of CD44 protein is significantly associated with poor primary therapy outcomes (progressive disease, stable disease, or partial remission/response), while low CD44 expression is associated with complete remission and response from primary therapy ($p = 0.056$, Welch's *t*-test, Fig. 1A Left). High ALDH1A3 protein expression was also significantly associated with poor primary therapy outcomes ($p = 0.011$, Welch's *t*-test, Fig. 1A Right). The combined score of ALDH1, CD44, and CD133 protein expression was significantly associated with poor primary therapy outcomes ($p = 0.009$, Welch's *t*-test).

3.1.2. Survival analysis of TCGA ovarian cancer cohort

Kaplan-Meier plots in Fig. 1B display the different overall survival of the patients with ovarian cancer with and without gene alterations. Overall survival analysis of the TCGA ovarian cancer cohort using cBioPortal revealed that patients with tumors harboring alterations (gene amplification, missense mutation, or overexpression of mRNA) in *ALDH1*, *CD44*, and *KIT* genes have worse survival outcome than patients whose tumors have no alternations in these genes ($p = 0.134$, log-rank test). Interestingly, about 8% of tumors harbored gene amplifications of *ALDH1*, *CD44*, or *CD117*. Another 20% of tumors overexpressed mRNA of ALDH1, CD44, or CD117.

3.2. HEY-T30 cells with high expression of CSC markers

Western blots were performed to evaluate the expression levels of CSC markers in HEY-T30, HCT 116, RKO, and HEK293 cells, and cancer-stem cell like properties of HEY-T30 cells were confirmed. As shown in Fig. 1C and D, HEY-T30 cells displayed higher expression levels of specific CSC markers (CD44, ALDH1A1, CD133, and CD117). CD44 expression of HEY-T30 cells was 96.9, 21.4, and 1.8 folds higher than that of HEK293, HCT 116, and RKO cells, respectively. These results are consistent with previous studies showing that CD44 is predominant in metastatic epithelial ovarian cancer (Alvero et al., 2011; Zhang et al., 2008). Additional migration assay (Fig. 1E) and colony forming assay (Fig. 1F) suggest that HEY-T30 is most invasive compared with the other cells.

3.3. Synthesis and physicochemical characteristics of PheoA-SN38-HC NPs

3.3.1. Preparation of PheoA-SN38-HC NPs

ROS-cleavable PheoA-SN38-HC NPs were successfully synthesized, as shown in Fig. 2. To prepare HC NPs, amine modified cholesterol was directly conjugated with HN to form the hydrophobic core of NPs, as described previously (Byeon et al., 2018). And HC NPs were further combined with photosensitizer (PheoA) to form PheoA-HC NPs (Fig. 2A left). Moreover, to introduce the ROS-cleavable drug to NPs, SN38-thioketal-NH_2 were additionally loaded to PheoA-SN38-HC NPs (Fig. 2D). Synthetic methods of ROS-cleavable diaminothioketal linker and SN38 drug conjugation were described in Supporting information Fig. S1. All compound synthesized step by step were analyzed by ^{1}H NMR and unique specific peaks of each material were identified as Supporting information Figs. S2, S3, and S4. As shown in the data, chemical shift (δ) of specific peaks were assigned as following; Compound **1**; δ 3.50 (2H,-CH_2-), 2.82 (2H,-CH_2-) and 1.50 ppm (1H,-SH) (Fig. S2A), compound **2**; δ 3.57 (2H,-CH_2-), 2.70 (2H,-CH_2-), and 1.59 ppm (3H,-CH_3) (Fig. S2B), compound **3**; δ 3.02 (2H,-CH_2-), 2.70 (2H,-CH_2-), and 1.59 ppm (3H,-CH_3) (Fig. S2C). In the case of PheoA-NH_2; δ 2.76 (2H,-CH_2-) and 3.66 ppm (3H,-CH_3) (Fig. S3A), SN38-thioketalamine; δ 3.02 (2H,-CH_2-) and 3.33 ppm (2H,-CH_2-) (Fig. S3B), SN38-hexamethylamine; δ 5.11 (2H,−NH_2) and 8.03 (1H,-NH-) (Fig. S3C), PheoA-HC; δ 3.46 (2H) and 3.66 (2H) (Fig. S4a), PheoA-SN38-(thioketal linker)-HC; δ 7.29 (1H, Benzene -CH) and 8.03 (1H, -NH-) (Fig. S4b).

3.3.2. Nanoparticle sizes and zeta potential

Particle sizes and morphologies of NPs were observed by transmission electron microscopy (TEM) and dynamic light scattering (DLS). As shown in TEM images of Fig. 2A right, all of nanoparticles were monodispersed and spherical shapes with the 200–300 nm range. The size of HC NPs (Fig. 2A a) was condensed and reduced by PheoA conjugation to HC nanoparticles, presumably due to the increased hydrophobicity of NP cores (Fig. 2A b). After SN38 conjugation to NP, surface morphology of nanoparticles became rough due to the SN38 attachment as shown in inserted enlarged TEM images of Fig. 2A c. In aqueous solution, the hydrodynamic sizes of HC NPs, PheoA-HC NPs, and PheoA-SN38-HC NPs were also measured to be 298 ± 43 nm (PDI = 0.431), 198 ± 65 nm (PDI = 0.332), and 263 ± 101 nm (PDI = 0.187), respectively (Fig. 2C), which were similar to size distribution of the TEM images. Additionally, zeta potential values of NPs were measured by to evaluate their surface condition and confirmed as −25.7 ± 5.73 mV (HC NPs), 18.3 ± 4.72 mV (PheoA-HC NPs), and 16.8 ± 5.9 mV (PheoA-SN38-HC NPs) due to the PheoA (ξ, PheoA itself = 21.5 ± 13.5 mV) and SN38 (ξ, SN38 itself = −19.4 ± 17.8 mV) conjugation.

3.3.3. Critical micelle concentration (CMC) of NPs

The critical micelle concentration (CMC) of HC NPs was also measured using a pyrene fluorescence probe, as previously described (Ray et al., 2006). The HC NPs introduced to hydrophobic cholesterol spontaneously formed micelle-like structures in aqueous solution, and the estimated CMC was 0.005 mg/ml (Fig. 2B).

3.3.4. Spectroscopic identification of drug conjugation

The sample images of Fig. 3A were obtained under visible and UV light (wavelength = 365 nm), which suggest the specific fluorescence properties of each NP. Engagement of PheoA and SN38 into NPs was confirmed via fluorescence and absorption spectra of NPs (Figs. 3B and S5). PheoA-HC NPs and PheoA-SN38-HC NPs showed strong fluorescence bands of PheoA and SN38/PheoA corresponding to SN38 (500–630 nm) and PheoA (600–800 nm), respectively (Fig. 3B). Absorption spectra showed the specific bands of PheoA at 400–450, 480–550, and 600–700 nm in PheoA-HC NPs, a broad SN38 absorption band at <400 nm, and PheoA absorption in PheoA-SN38-HC NPs (Fig. S5). The PheoA and SN38 contents of nanoparticles were calculated by measuring absorbance at 670 nm (free PheoA) or 380 nm (free SN38), and were measured to 1.08 and 1.21 w%, respectively.

3.4. In vitro photodynamic ROS generation and ROS-triggered SN38 release

3.4.1. 670 nm NIR-responsive photodynamic ROS generation

NIR-responsive photodynamic singlet oxygen generation of NPs was estimated under NIR irradiation with the presence of a fluorescent probe (9, 10-dimethylanthracene, DMA). DMA is transformed into non-fluorescent endoperoxide anthracene under singlet oxygen and allows estimation of ROS generation capacity of PheoA-SN38-HC NPs (Martins

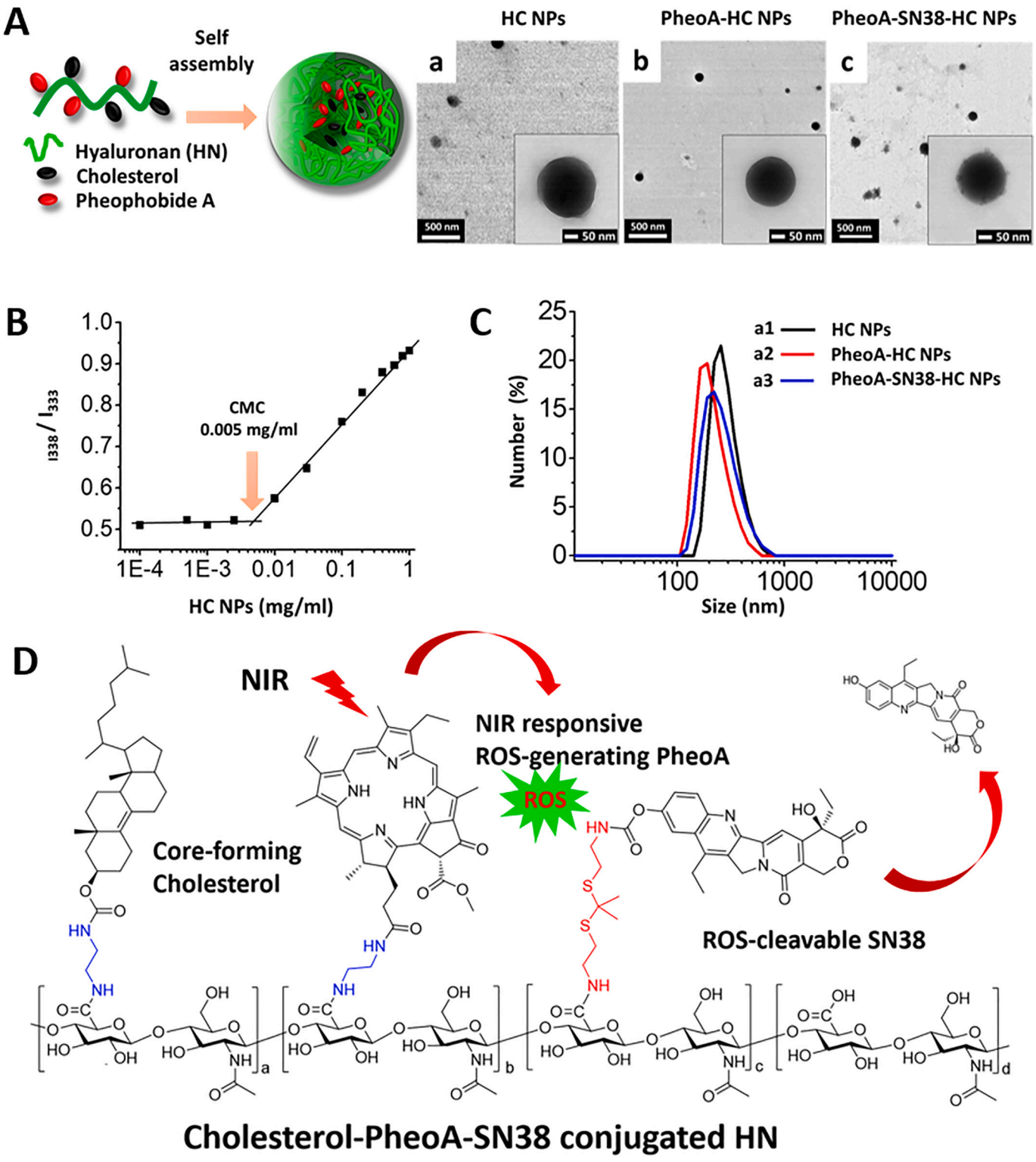

Fig. 2. Preparation of PheoA-SN38-HC NPs with combination therapeutic design; A. Self-assembled PheoA-HC NPs and TEM images of NPs. B. CMC value for HC NPs; Plots of I_{338}/I_{333} ratio vs. concentration of HC NPs. Pyrene in acetone (30 mM) was diluted with distilled water to 1.2 μM. Then, HC NPs at various concentrations from 0.001 to 1 mg/ml was mixed with pyrene solution at a 1:1 volume ratio. The excitation spectra of pyrene (300–360 nm, emission 390 nm) were obtained using a fluorometer (Infinite M200 Pro, Tecan) and the CMC was determined by plotting the ratio of intensity at wavelengths of 338 and 333 nm versus the HC NPs concentration. CMC value of HC NPs = ~0.005 mg/ml. C. hydrodynamic sizes of NPs. D. Schematic structure of HC-PheoA-SN38 NPs for PDT and controlled drug release.

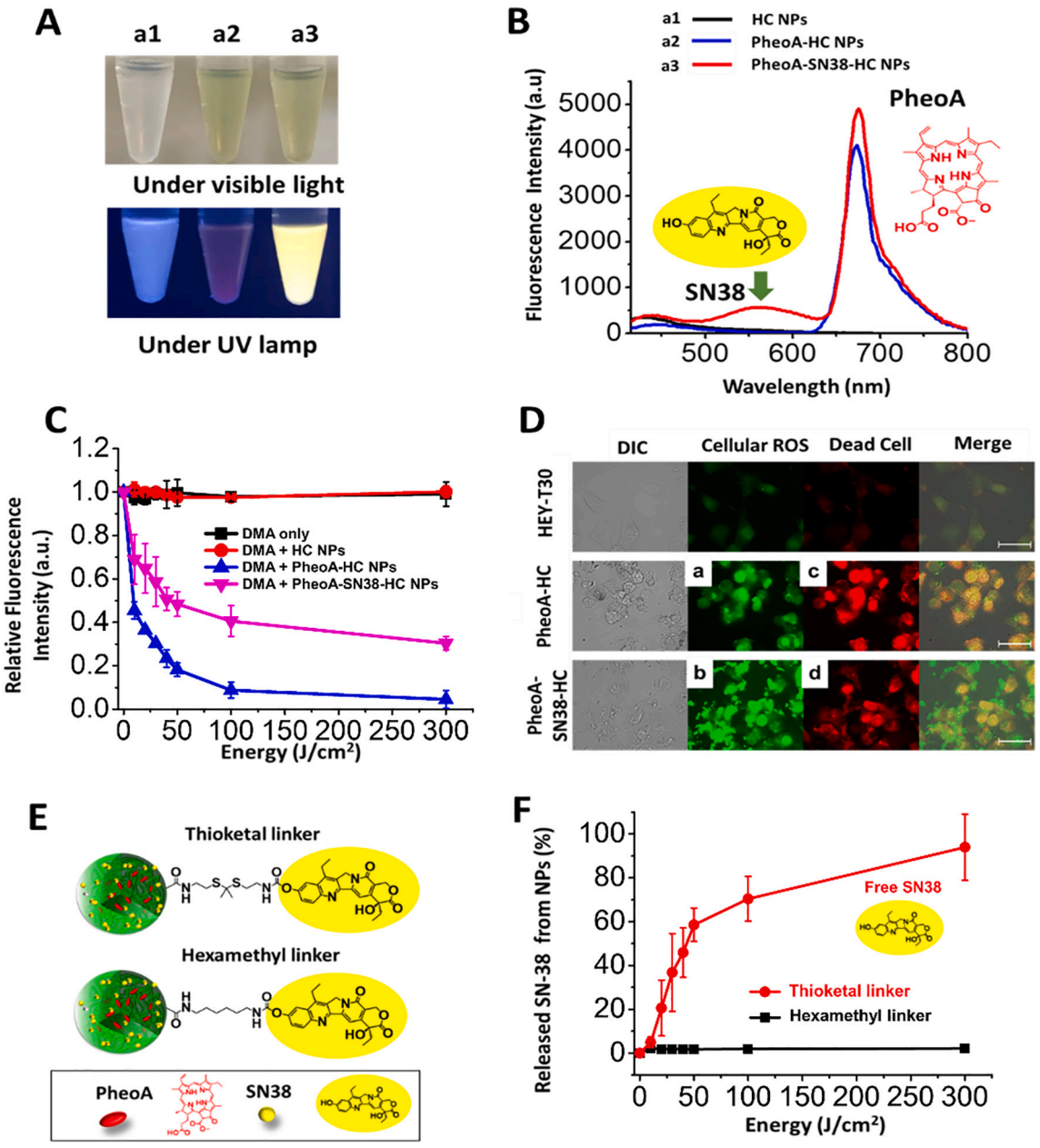

Fig. 3. Characterization of PhoeA-SN38-HC NPs; A. Photo images of HC NPs, PheoA-HC NPs, and PheoA-SN38-HC NPs. B. Fluorescence spectra of NPs. C. NIR induced singlet oxygen generation from NPs. In the presence of DMA (100 μM), 1 mg/ml NPs were exposed to light, and fluorescence intensity (λ = 420 nm) of DMA was measured by spectrometer. D. Fluorescence microscopic images of HEY-T30 cells with NPs (Final conc. 0.2 mg/ml) + SOSG (singlet oxygen sensor green) after NIR irradiation (100 J/cm^2). Scale bar = 50 μm. E. Structures of ROS-cleavable thioketal linker modified PheoA-SN38-HC NPs and non-cleavable hexamethyl linker modified PheoA-SN38-HC NPs. F. Light induced drug release from NPs depending on light energy.

et al., 2014). NP solutions containing DMA were irradiated with 0–300 J/cm^2 laser light, and the fluorescence intensity of DMA at 430 nm was measured. As shown in Fig. 3C, the relative DMA fluorescence intensities of PheoA-HC and PheoA-SN38-HC samples decreased with increasing NIR energy, but HC NPs did not show a change in fluorescence. This finding indicates that PheoA loaded HC NPs generate singlet oxygen in an NIR energy-dependent manner.

In the case of PheoA-SN38-HC NPs, ROS generation efficiency was slightly lower than that of PheoA-HC NPs. This result is thought that some of ROS produced by PheoA are partially reabsorbed for the thioketal linker cleavage.

Similarly, intracellular ROS accumulation with PheoA-HC NPs or PheoA-SN38-HC NPs was observed via SOSG fluorescence staining (Fig. 3D). HEY-T30 cells treated with PheoA-HC NPs or PheoA-SN38-HC NPs showed strong green SOSG fluorescence under NIR irradiation. Specifically, dead cell staining (red fluorescence produced by ethidium homodimer-1, Fig. 3D c and d) suggests that ROS generation by PheoA-HC NPs or PheoA-SN38-HC NPs is strong enough to induce cell death.

3.4.2. *ROS-responsive cascadic release of SN38*

As previously mentioned, PheoA-SN38-HC NPs were designed to generate ROS under NIR-irradiation and then release SN38 from ROS-induced cleavage of thioketal linkers (Fig. 2D). To evaluate the controlled drug release property of NPs, two types of PheoA-SN38-HC NPs were prepared, one with a ROS-cleavable thioketal linker and the other with a non-cleavable hexamethyl linker (Fig. 3E). As shown in Fig. 3F, the SN38 released from ROS-cleavable PheoA-SN38-HC NPs increased with increasing NIR exposure and saturated at 300 J/cm^2.

However, SN38 release was not observed from non-cleavable hexamethyl linker modified PheoA-SN38-HC NPs under any NIR irradiation. This result clearly shows that the thioketal linker is an effective structure for ROS-sensitive controlled drug release.

3.5. Cytotoxic effects of PheoA-SN38-HC NPs on chemo-resistant HEY-T30 cells

3.5.1. CD44 target specific uptake of PheoA-SN38-HC NPs

As shown in a previous study (Figs. 1C and 4D), the expression of CSC markers in HEY-T30 cells was clearly observed via western blot assay. Additionally, FACS analysis was also performed to prove overexpression of CD44 in HEY-T30 cells. As shown in Fig. S6, FITC-CD44 antibody staining FACS analysis revealed that the CD44 expression level of HEY-T30 was much higher than that of other cells (HEK293, RKO, and HCT116 cells).

To evaluate the CD44 target specificity of NPs, HEY-T30 cells were incubated with PheoA-HC NPs or PheoA-SN38-HC NPs with or without the CD44 blocking control. Then, CD44 binding and cellular uptake of NPs were analyzed by FACS or confocal microscopy. Based on FACS data (Fig. 4A), the uptake of PheoA-HC NPs by CD44 unblocked cells was 8-fold higher than that of CD44 blocked cells (mean fluorescence intensity value, 212 A.U. for blocked vs. 1702 A.U. for non-blocked). CD44 target specificity was also confirmed via fluorescence microscopic observation. HA-pretreated (CD44 blocked) cells showed much lower fluorescence of PheoA (red) and SN38 (green) of PheoA-SN38-HC NPs (or PheoA-HC NPs) (Fig. 4B).

Dual drug uptake by HEY-T30 cells was visualized via confocal microscopic images of PheoA and SN38 of NPs (Fig. 5A). In the NIR non-irradiation, HEY-T30 cells treated with PheoA-HC NPs or PheoA-SN38-HC NPs showed strong red and red/green fluorescence in cytoplasm, respectively, whereas non-treated control and HC NP treated cells showed no fluorescence. After NIR irradiation, fluorescence intensities of red channels (PheoA) in PheoA-HC NP and PheoA-SN38-HC NP treated cells were slightly reduced due to photobleaching of PheoA. In particular, strong green/red fluorescence overlap (yellow dots in merged images of PheoA-SN38-HC NPs treatment) of non-NIR condition disappeared after NIR irradiation, which is thought that the SN38 was detached and released from NPs.

3.5.2. Combination cytotoxicity of photodynamic ROS and ROS-trigger released SN38

Light-responsive cytotoxic effects of PheoA-SN38-HC NPs were evaluated against HEY-T30 cells. Fig. 5B shows that each NP (HC NPs, PheoA-HC NPs, or PheoA-SN38-HC NPs) in the concentration range of 5–50 μg/ml did not affect cell viability (≥80% cell viability). Fig. 5C also shows that control HEY-T30 cells and HC NPs treated HEY-T30 cells without light maintained cell viability. However, light irradiation at a power of 100 J/cm^2 in HEY-T30 cells after PheoA-HC and PheoA-SN38-HC treatment was cytotoxic enough to reduce cell viability to ~20% and ~10%, respectively. However, the cytotoxic combination effect was not detectable in this study because of the strong cytotoxic effect of photodynamic treatment itself.

3.5.3. Paracrine cytotoxic effects of ROS-trigger released SN38

Photodynamic treatment is only effective on light-penetrated region. Our PheoA-SN38-HC NPs release SN38 under photodynamic ROS-triggering, and the released SN38 smears to the surrounding tumor tissues and displays paracrine cytotoxic effects. Paracrine cytotoxic effects of SN38 were observed as bellow. HEY-T30 cells were incubated with PheoA-HC NPs or PheoA-SN38-HC NPs in 8-well chambered glass for 4 h. Then, the left half of HEY-T30 cells was irradiated by NIR light with 100 J/cm^2, co-stained with Calcein AM (for live cell staining, green) and ethidium homodimer-1 (for dead cell staining, red), and observed under a fluorescence microscope. As shown in Fig. 6A of the live/dead cell staining images, most of the laser-nontreated area showed green fluorescence (live cells; a, b, d, e, f and h). The photodynamic activities of each NP were observed on c (c′) and g (g′) regions (c and g; non-green for live cell imaging, c′ and g′; strong red for dead cell imaging). However, laser-nontreated and NP-nontreated h (h′) regional cells were badly damaged and showed strong red fluorescence (h′) without green fluorescence (h). These results strongly suggest that the paracrine release effect of SN38, that is, the SN38 released from PheoA-SN38-HC NPs of the E region after NIR-treatment, smeared to the h (h′) region and disserted a cytotoxic effect (h′; red fluorescence for dead cells). The fluorescence intensity of live/dead cell staining images was measured using ImageJ program, and the results are displayed in Fig. 6B and C. The cellular area without any treatment (Fig. 6, region of h and h′) showed higher intensity of red fluorescence (Fig. 6C, dead cells) and relatively low green intensity of live cells (Fig. 6B, live cells). These results suggest

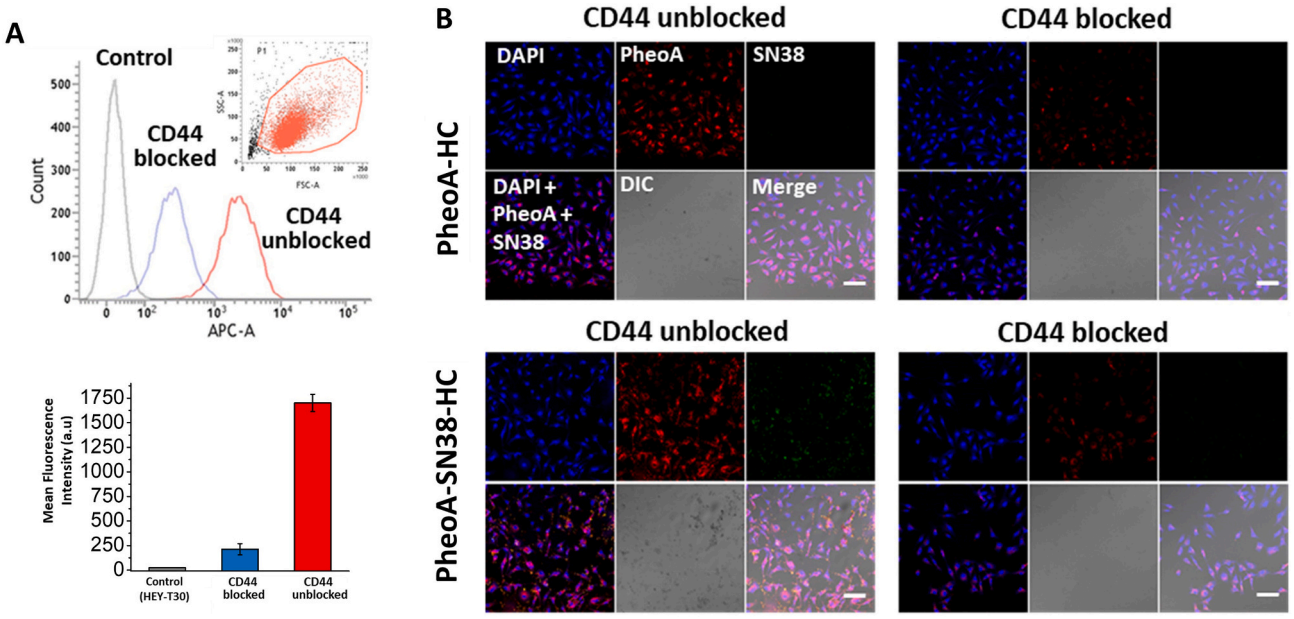

Fig. 4. Cellular uptake of NPs; A. FACS data of HEY-T30 incubated with PheoA-HC NPs with/without HA pretreatment (up) and mean fluorescence intensity graphs (down). B. Confocal microscopic images of PheoA-HC and PheoA-SN38-HC NPs treated HEY-T30 cells. Scale bar = 100 μm.

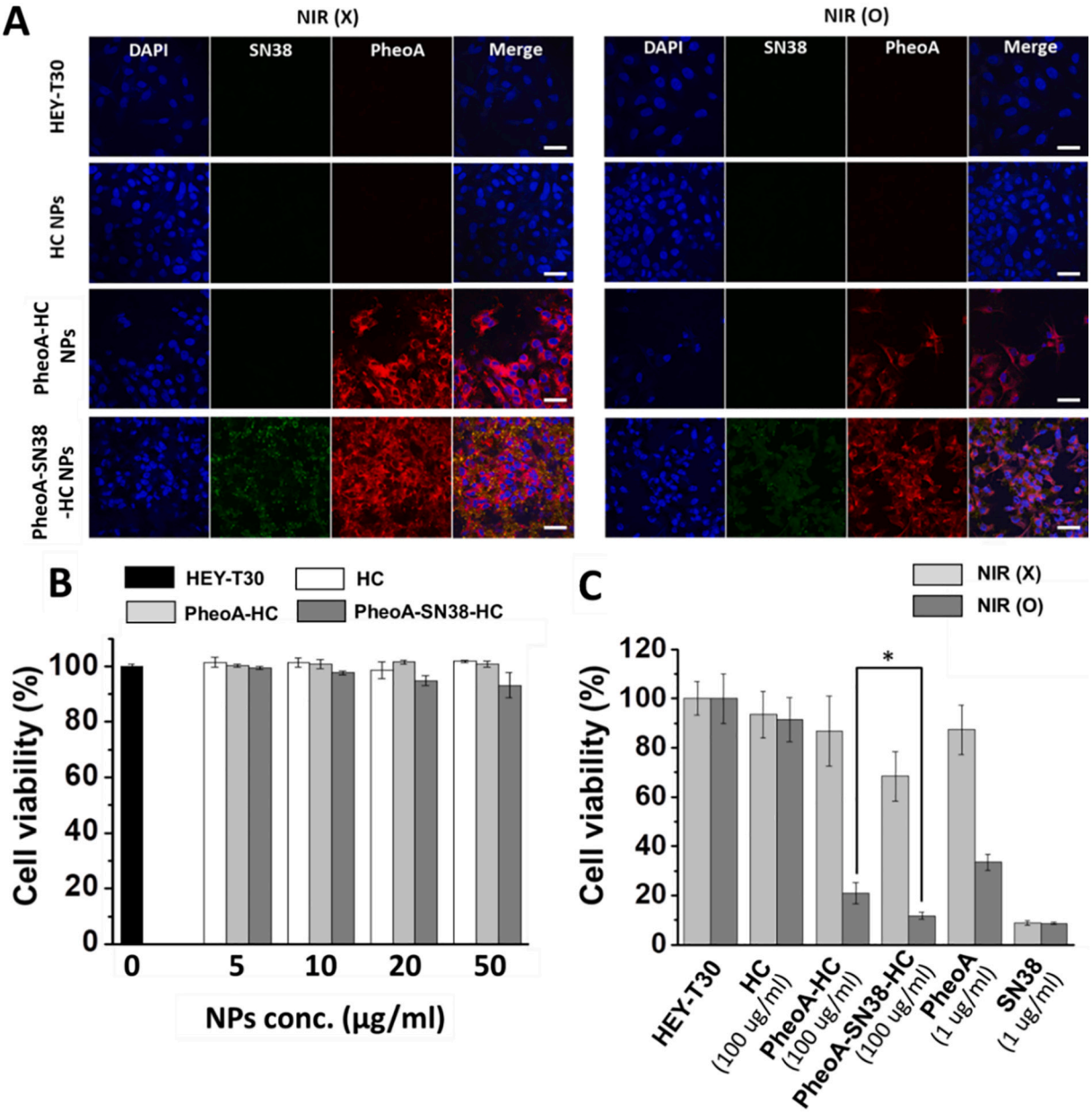

Fig. 5. Cellular uptake and toxicity; A. Confocal microscopic images of HEY-T30 treated with NPs w/wo light. B. Concentration dependent cell viability of NPs (NPs concentration = 0, 5, 10, 20, 50 μg/ml). After 24 h incubation in the absence of light, cell viability test was performed. B. Cell viability at light exposure/non-exposure condition; NPs concentration = 100 μg/ml, incubation time = 24 h, light (O) = 167 m W/cm^2, 10 min. *$P < 0.05$ by the Student's *t*-test.

that SN38 released from photo-treated PheoA-SN38-HC NPs travelled to other chambers and displayed a paracrine cytotoxic effect.

3.6. *In vivo tumor targeting of PheoA-SN38-HC NPs*

In vivo tumor targeting properties of NPs were evaluated in HEY-T30 xenografted BALB/c nude mice. Two weeks after subcutaneous injection of HEY-T30 into mice, red fluorescent dye, Cy5, labeled HC NPs were injected into mouse tail vein. As blocking experiment, HN was pre-injected before Cy5-HC NPs. As shown in in vivo fluorescence images at 72 h after NPs injections of Fig. 7A, strong red fluorescence of Cy5-HC NPs was accumulated in tumor region, but HN + Cy5-HC NPs were not detected (Fig. 7A). To confirm the in vivo NPs distribution, each organ (heart, lung, spleen, liver, kidney, and HEY-T30 tumor) was extracted from mice, their fluorescence images were obtained, and the relative fluorescence intensity was measured (Fig. 7B). As shown in Fig. 7B fluorescence intensity graph of organs, fluorescence intensity of tumor region in Cy5-HC NPs treated sample was ~2.5 times greater than that of HN + Cy5-HC NPs treated sample. From this result, HC NPs showed the targeting property to in vivo HEY-T30 tumor as well as in vitro. Moreover, extracted tumors were further analyzed by confocal microscopy to find the NPs (Fig. 7C). After tumor sectioning by cryotome, tumors were further stained with DAPI. As shown in the images of Fig. 7C, Cy5-HC NPs treated samples clearly showed the red fluorescent dots in the tumor region.

3.7. *In vivo therapeutic efficacy of combination NPs*

The in vivo therapeutic efficacy of PDT and chemotherapy of PheoA-SN38-HC NPs were also investigated. After tumor growth to ~100 mm^3 in the subcutaneous mouse model, the same amounts of HC NPs, PheoA-HC NPs, or PheoA-SN38-HC NPs (dosage 10 mg/kg) were intratumorally

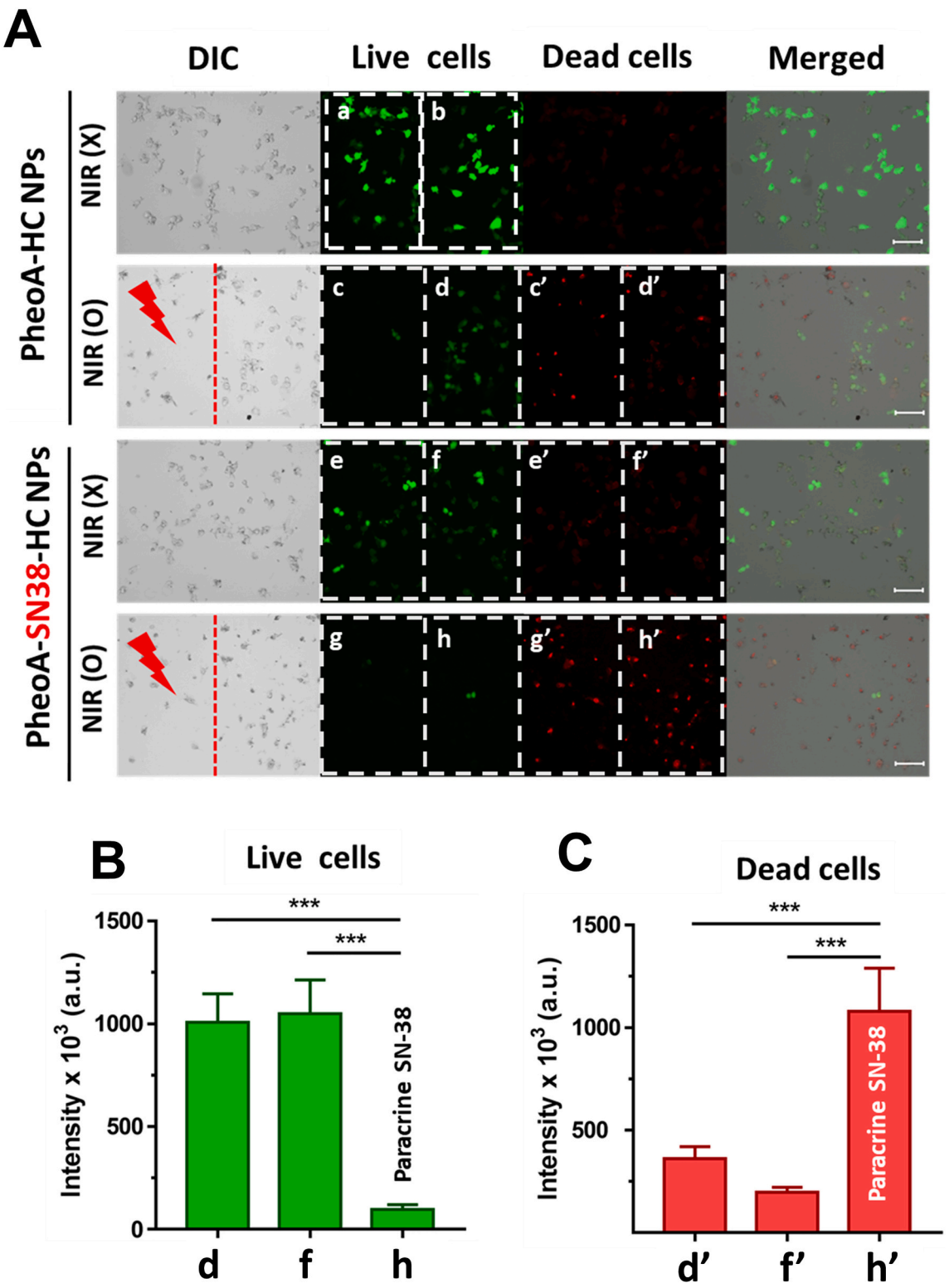

Fig. 6. Paracrine effect of ROS-trigger released SN 38; A. Confocal microscopic images with local irradiation of light into NPs treated HEY-T30 cell. All cells were stained with Calcein AM (green, live cells) and Ethidium homodimer-1 (red, dead cells). Positive red staining (panel c′ and panel g′) of HEY-T30 cells after light exposure shows photodynamic cytotoxic effect of PheoA-HC NPs and PheoA-SN38-HC NPs. Positive red staining of light blocked region (panel h′) implies cytotoxicity of the ROS-cleavable SN38 after light treatment of PheoA-SN38-HC NPs. Scale bar = 100 μm. B. Relative fluorescence intensity of Calcein AM (live cells) in light non-exposed regions (D, F, and H) of A. C. Relative fluorescence intensity of ethidium homodimer-1 (dead cells) in NIR non-exposed regions (d′, f′, and h′) of A. ***$P <$ 0.001 by the Student's *t*-test.

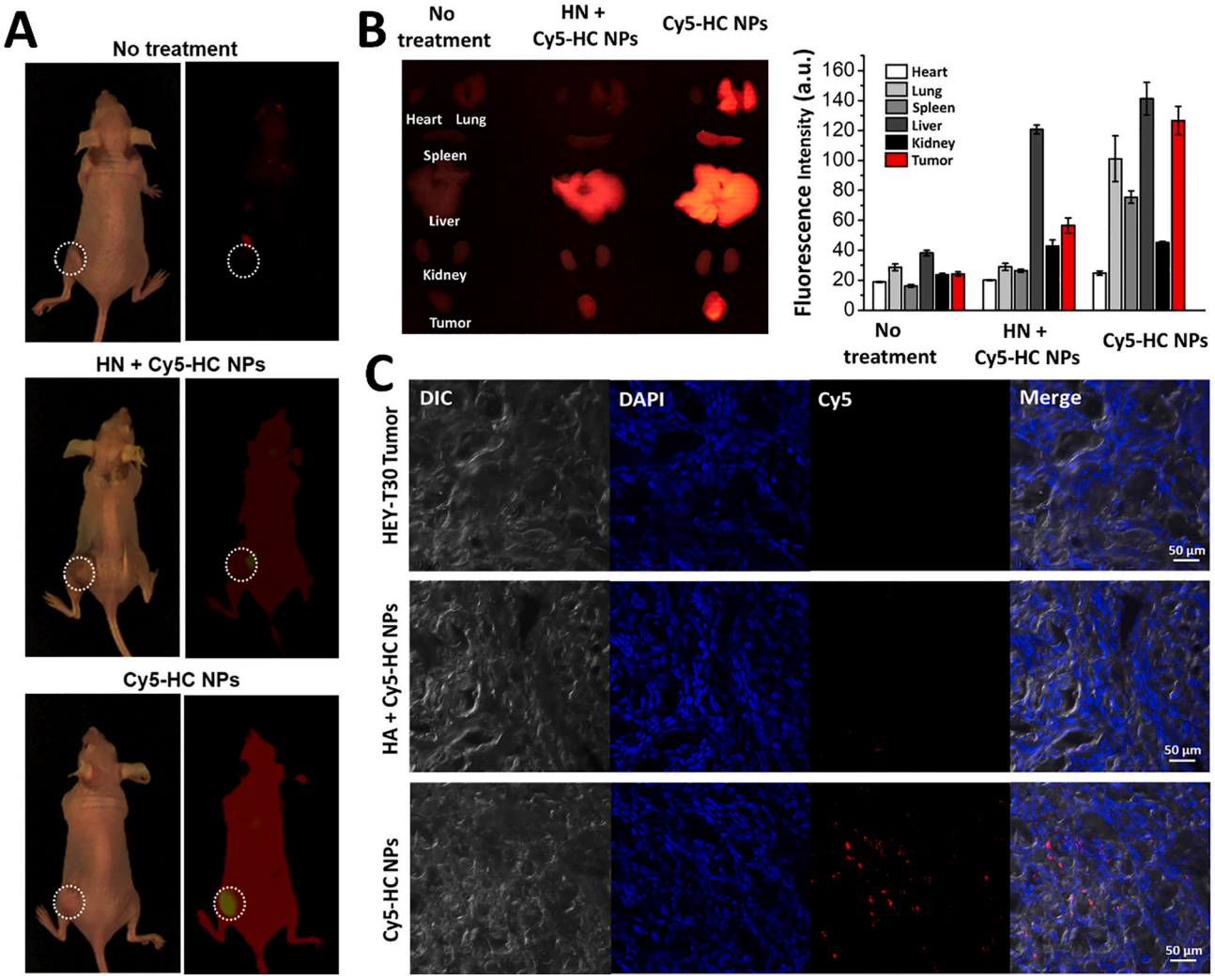

Fig. 7. In vivo tumor targeting of NPs. A. HEY-T30 xenograft BALB/C nude mice were injected with NPs (1 mg/kg) into tail vein and fluorescence images were obtained after 72 h; As blocking experiment, HN (1 mg/kg) was pre-injected 30 min before NPs treatment. In vivo imaging instrument: FOBI (NEO Science, South Korea). B. Fluorescence images of organs (heart, lung, spleen, liver, kidney, and tumor) harvested after 72 h (Left) and relative fluorescence intensity of tissues analyzed by ImageJ software (Right). C. Confocal microscopic images of extracted HEY-T30 tumors; Each tumor was sectioned to 50 μm thickness by cryotome and further stained with DAPI.

injected. Tumors were irradiated with 671 nm light (100 J/cm^2) once a day for three consecutive days, and tumor volumes and body weights were measured for a month. Body weights in the treatment groups were similar (Fig. 8A). Tumor volumes gradually increased over time in the non-irradiated PBS, PheoA-HC, and PheoA-SN38-HC groups (Fig. 8B). In the NIR exposed PheoA-HC NP treated group on the 28th day, tumor growth was inhibited by ~55% compared with the PBS group. The NIR irradiated PheoA-SN38-HC NP group showed greater therapeutic efficacy (~70% less tumor volume in PBS group on the 28th day). In addition, H&E staining and TUNEL images obtained after extraction of light irradiated tumors (Fig. 8C) revealed higher levels of apoptosis and necrosis in the PheoA-HC and PheoA-SN38-HC treated groups than in PBS or HC NP treated groups. PheoA-SN38-HC treated sample images showed the highest tumor damage, suggesting a synergistic tumor suppression effect of PDT/chemo combination therapy. Additionally, toxicity was further investigated the toxicity through H&E staining of major organs including liver, lung, heart, kidney, and spleen extracted from mouse treated with various nanoparticles. As shown in SI Fig. S7, there was no toxic effect in each organ, and it was confirmed the safety of nanoparticles from these results.

4. Discussion

4.1. Clinical implication of CSC markers in prognosis of OC

From CPTAC proteome data, we observed correlation with the expression of CSC markers in OC tissues and poor primary therapy outcomes. Fig. 1A suggests that the ovarian CSC population, especially for CD44 and ALDH1A1, is responsible for poor responses to primary therapy. Moreover, the worse overall survival of patients with genetic alterations in ovarian CSC marker genes implies that stemness of ovarian cancer cells may be a factor contributing to the overall survival of patients with ovarian cancer (Fig. 1B). Additionally, we observed mRNA expression levels of stem cell markers in ovarian tumor samples and normal ovary tissues using The Cancer Genome Atlas TCGA datasets (TCGA) and Genotype-Tissue Expression Portal datasets (GTEx) (refer to Supplemental information). The results showed that ovarian stem cell markers (mRNA of *CD44*, *EPCAM*, *PROM1*, and *CD24*) were significantly overexpressed in ovarian cancer tumors compared to normal ovary tissues (Fig. 9A).

Among CSC markers, CD44 and ALDH1A1 have been for therapeutic targets of OC treatment. Yanqing et al. reported that CD44 is a controlling factor for ovarian cancer cell invasion, migration, and colony

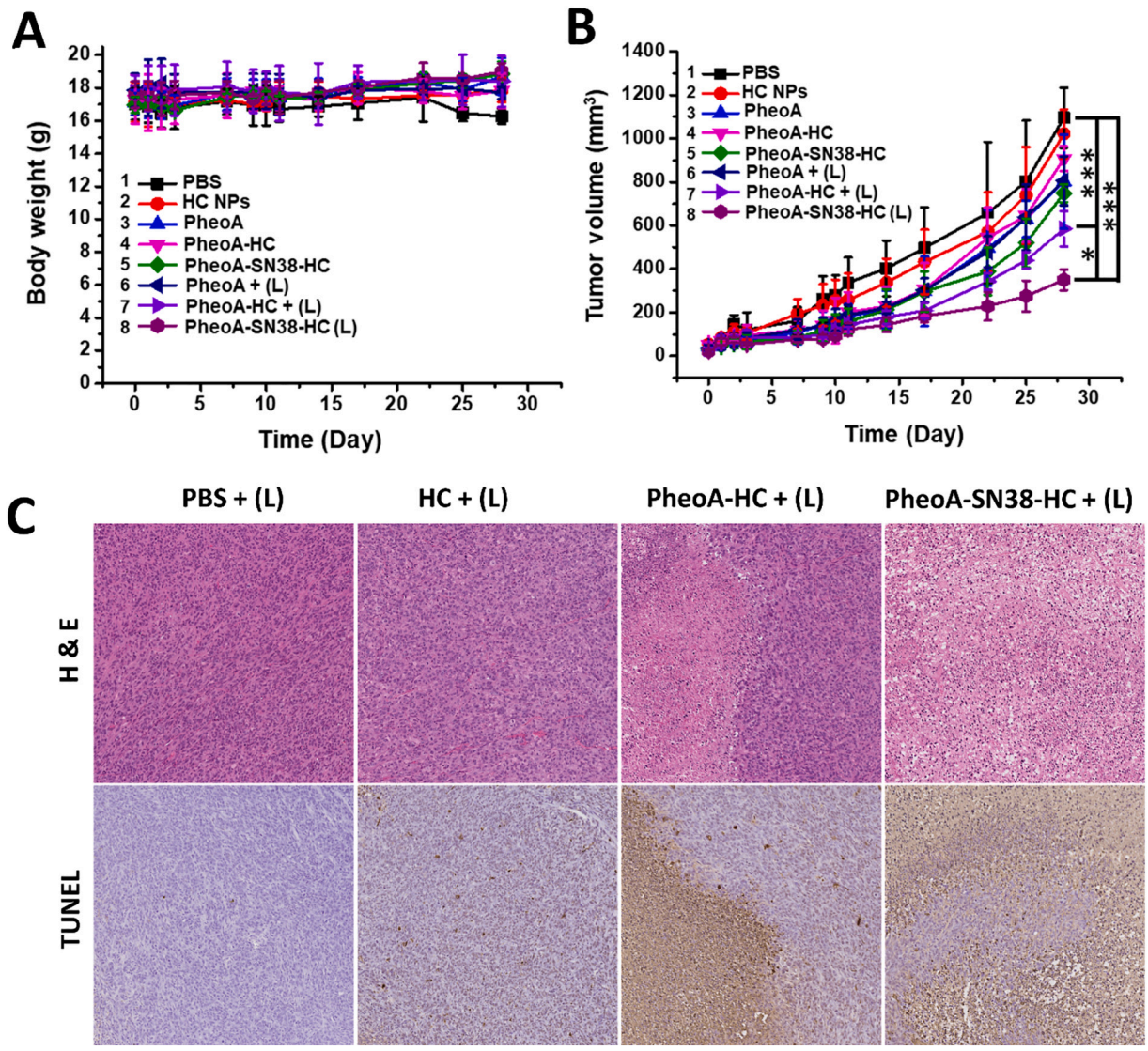

Fig. 8. In vivo PDT treatment with HC-PheoA-SN38. Body weights (A) and tumor growth curves (B) of HEY-T30 xenograft BALB/C nude mouse. Data are shown as the mean values ± SD ($n = 5$); *$p < 0.05$, ***$P < 0.001$ by the Student's *t*-test. C. H&E and TUNEL stained tumor slices obtained at day 28.

formation (Wang et al., 2019). Landen et al. reported that 72.9% of ovarian cancer patient samples expressed ALDH1A1 and negatively correlated with progression-free survival (expressed vs non-expressed; 6.05 vs. 13.81 months; $P < 0.035$) (Landen et al., 2010). ALDH1A1 is significantly related to chemo- (taxane and platinum) resistance and poor patient survival (Kaipio et al., 2020; Landen et al., 2010). Our western blot data proved that HEY-T30 shows 1.9–12.9 folds higher expression of ALDH1A1 than other cells. Interestingly, HEY-T30 is 40-fold more resistant to paclitaxel (IC50: 2.6 nM vs. 105.9 nM) (Brouwer-Visser et al., 2014b). Therefore, we suggest that co-expression of CD44 and ALDH1A1 is highly related to the invasive and chemo-resistant stem cell-like properties of HEY-T30.

4.2. 'Pan-CSC marker' target therapy

As observed with CPTAC proteome data and other reports, the CSC markers CD44, ALDH1A1, and CD117, are major target proteins for therapeutic system design (Ayob & Ramasamy, 2018; Tao et al., 2018). However, successful 'pan-CSC' targeting therapy is difficult because of the heterogeneity of CSCs. Among CSC markers, CD44 has recently been identified as an ovarian CSC marker (Browning et al., 2017; Byeon et al., 2018).

CD44 has been studied as a therapeutic target moiety in designing nano therapeutic systems (Byeon et al., 2018), but it has not been studied as extensively for CSC targeting nanoparticles to overcome drug-resistant and metastatic properties. Conversely, folate receptor has been extensively utilized for ovarian cancer target therapy (Nie et al., 2018). Our study on mRNA expression levels of OC samples also proved that mRNA of folate receptor (*FOLR1*) and *CD44* is significantly overexpressed in ovarian cancer tumors ($p = 7e\text{-}27$ and $p = 3e\text{-}8$, respectively) (Fig. 9B). However, high expression of *FOLR1* mRNA is inversely correlated with OC progression ($p = 0.017$) compared with *CD44* mRNA ($P = 0.056$) (Fig. 9C). Recently, Norton and his research group reported folate receptor alpha expression associates with improved disease-free survival in triple negative breast cancer patients (Norton et al., 2020). Therefore, our observation suggests that CD44, rather than folate receptor, might be a reasonable therapeutic target design, especially for metastatic and chemo-resistant OC treatments. Therefore, we applied a CD44 targeting system as a 'pan-CSC' targeting therapy in combination design of photodynamic and chemotherapy.

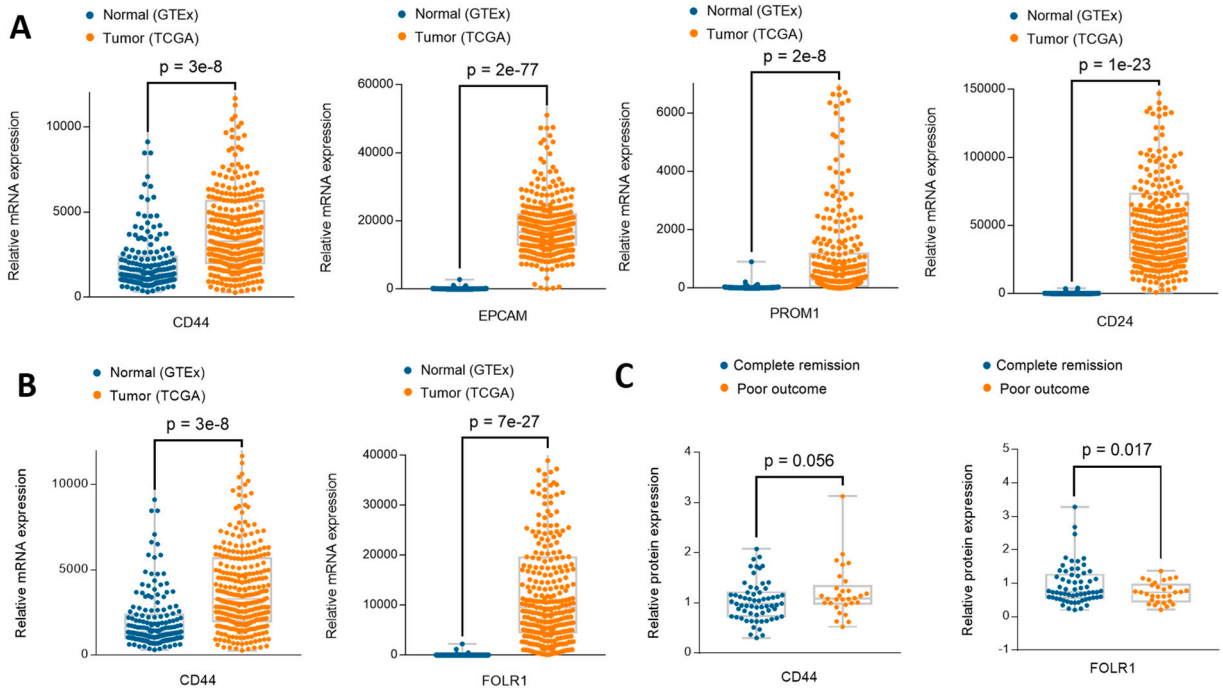

Fig. 9. Clinical relevance of CSC marker gene and proteins expression in ovarian cancer patient tissues. A. Relative mRNA expression level of *CD44*, *EPCAM*, *PROM1*, and *CD24* in in normal ovary tissues (GTEx) and ovarian cancer tumor samples (TCGA). B. Relative mRNA expression levels of *CD44* and *FOLR1* in GTEx and TCGA. C. Relative protein expression levels of CD44 and FOLR1 in complete remission and poor outcome. GTEx and TCGA data suggest mRNA of *CD44* and *FOLR1* is highly expressed in ovarian tumor tissues rather than normal ovarian tissues. However, data show protein expression of CD44 highly correlated with poor progress outcome in OC patients.

4.3. NIR-responsive photodynamic and chemotherapeutic combination therapeutic system

Combination chemotherapy, which combines two or more therapeutic agents, has now become the standard therapeutic regimen. Combination chemotherapy targets several cancer pathways in a typically synergistic or additive manner to enhance therapeutic efficacy and patient survival (Holohan et al., 2013; Longley & Johnston, 2005; Swanton, 2012). Photodynamic therapy (PDT), which principally works by systemic injection of photosensitizers and laser-induced activation, is one of the best therapeutic modalities for combination chemotherapy because PDT does not cause systemic side effects compared to conventional chemotherapy (Baskaran et al., 2018). However, most tumor tissues grow deep inside organ tissues, where NIR cannot reach; therefore, NIR may fail to induce total death or apoptosis of tumor cells (Mallidi et al., 2016). More selective and functional design of photosensitizers that respond to low dose photoenergy are of great interest to achieve complete tumor regression.

Our data suggest that combination therapeutic design, such as that offered by PheoA-SN38-HC, exhibits more enhanced therapeutic effects due to ROS-triggered SN38 release design. In particular, the paracrine cytotoxic effect of SN38 from PheoA-SN38-HC NPs might overcome the critical defects of photodynamic laser therapy (Fig. 6).

In vivo efficacy results corresponded with an in vivo study performed against HEY-T30 xenograft cancer on a mouse model. Fig. 7 shows that the PheoA-SN38-HC NP group significantly inhibited cancer growth (~70% less tumor volume in PBS group on the 28th day), compared with the PheoA-HC NPs group, PheoA-SN38-HC NPs group, and non-treated group.

PheoA-SN38-HC NPs with photodynamic and ROS-cleavable SN38 therapy clearly showed improved CD44 positive cancer targeting efficiency and anticancer effects through in vitro and in vivo studies. These results strongly imply that CD44 can be applied for pan-CSC.

5. Conclusion

In summary, photosensitive, ROS-cleavable PheoA-SN38-HC NPs were designed and prepared. To realize combined PDT/chemotherapy for cancer, SN38 was attached to HN-based nanoparticles using a highly sensitive ROS-cleavable thioketal linker. By utilizing the ROS generated by the photosensitizer Pheophorbide A, SN38 was released by PheoA-SN38-HC NPs exposed to NIR laser light. To identify an appropriate tumor model, CD44 expression levels were investigated in several human cancer cell lines by flow cytometry, and the HEY-T30 cell line was selected for the study. The cancer specific binding property of NPs, potential efficacy of PDT, and NIR-induced release of SN38 from PheoA-SN38-HC NPs were assessed in vitro by flow cytometry and cellular imaging. PheoA-SN38-HC NPs had a marked tumor suppressive effect in the HEY-T30 tumor xenograft BALB/c nude mouse model.

CRediT authorship contribution statement

Junghan Lee: Data curation, Investigation, Methodology, Writing – Original draft, Funding acquisition.
Enkhzaya Davaa: Investigation.
Yixin Jiang: Investigation.
Kyung-Ju Shin: English edition.
Min Hye Kim: Investigation, Chemical synthesis.
Hyunsu An: Investigation, CPTAC data acquisition and validation.
Jinho Kim: Resources, Investigation, Chemical synthesis.
Steve K. Cho: Investigation, Data validation.
Su-Geun Yang: Resources, Supervision, Writing – review & editing, Funding acquisition.

Declaration of competing interest

The authors have declared that no competing interest exists.

Acknowledgements

This work was supported by the Basic Science Research Program and the Bio & Medical Technology Development Program of the National Research Foundation (NRF) funded by the Korean government (MOE and MSIT) (2020R1I1A1A01073559, 2020R1A2B5B02002377, 2018R1A6A1A03025523, and 2019M3E5D1A02069623).

Availability of data and materials

The data generated during the experiments has been reported in manuscript.

Appendix A. Supplementary data

Supplementary data to this article can be found online at https://doi.org/10.1016/j.carbpol.2022.119455.

References

Alvero, A. B., Montagna, M. K., Holmberg, J. C., Craveiro, V., Brown, D., & Mor, G. (2011). Targeting the mitochondria activates two independent cell death pathways in ovarian cancer stem cells. *Molecular Cancer Therapeutics, 10*(8), 1385–1393.

Angeles, G. H., & Nesporova, K. (2021). Hyaluronan and its derivatives for ophthalmology: Recent advances and future perspectives. *Carbohydrate Polymers, 259*.

Arbour, K. C., & Riely, G. J. (2019). Systemic therapy for locally advanced and metastatic non-small cell lung cancer a review. *Jama-Journal of the American Medical Association, 322*(8), 764–774.

Ayob, A. Z., & Ramasamy, T. S. (2018). Cancer stem cells as key drivers of tumour progression. *Journal of Biomedical Science, 25*.

Baskaran, R., Lee, J., & Yang, S. G. (2018). Clinical development of photodynamic agents and therapeutic applications. *Biomaterials Research, 22*, 25.

Brouwer-Visser, J., Lee, J., McCullagh, K., Cossio, M. J., Wang, Y., & Huang, G. S. (2014a). Insulin-like growth factor 2 silencing restores taxol sensitivity in drug resistant ovarian cancer. *PLoS One, 9*(6), Article e100165.

Brouwer-Visser, J., Lee, J., McCullagh, K., Cossio, M. J., Wang, Y. H., & Huang, G. S. (2014b). Insulin-like growth factor 2 silencing restores taxol sensitivity in drug resistant ovarian cancer. *Plos One, 9*(6).

Browning, R. J., Reardon, P. J. T., Parhizkar, M., Pedley, R. B., Edirisinghe, M., Knowles, J. C., & Stride, E. (2017). Drug delivery strategies for platinum-based chemotherapy. *ACS Nano, 11*(9), 8560–8578.

Byeon, Y., Lee, J. W., Choi, W. S., Won, J. E., Kim, G. H., Kim, M. G., & Park, Y. M. (2018). CD44-targeting PLGA nanoparticles incorporating paclitaxel and FAK siRNA overcome chemoresistance in epithelial ovarian cancer. *Cancer Research, 78*(21), 6247–6256.

Carioli, G., Malvezzi, M., Bertuccio, P., Hashim, D., Waxman, S., Negri, E., & La Vecchia, C. (2019). Cancer mortality in the elderly in 11 countries worldwide, 1970–2015. *Annals of Oncology, 30*(8), 1344–1355.

Debeb, B. G., Zhang, X. M., Krishnamurthy, S., Gao, H., Cohen, E., Li, L., & Woodward, W. A. (2010). Characterizing cancer cells with cancer stem cell-like features in 293T human embryonic kidney cells. *Molecular Cancer, 9*.

Gao, J. J., Aksoy, B. A., Dogrusoz, U., Dresdner, G., Gross, B., Sumer, S. O., & Schultz, N. (2013). Integrative analysis of complex cancer genomics and clinical profiles using the cBioPortal. *Science Signaling, 6*(269).

Gomes, A., Fernandes, E., & Lima, J. (2005). Fluorescence probes used for detection of reactive oxygen species. *Journal of Biochemical and Biophysical Methods, 65*(2–3), 45–80.

Gottesman, M. M. (2002). Mechanisms of cancer drug resistance. *Annual Review of Medicine, 53*, 615–627.

Govindan, S. V., Cardillo, T. M., Sharkey, R. M., Tat, F., Gold, D. V., & Goldenberg, D. M. (2013). Milatuzumab-SN-38 conjugates for the treatment of CD74 cancers. *Molecular Cancer Therapeutics, 12*(6), 968–978.

Holohan, C., Van Schaeybroeck, S., Longley, D. B., & Johnston, P. G. (2013). Cancer drug resistance: An evolving paradigm. *Nature Reviews Cancer, 13*(10), 714–726.

Huang, G. S., Brouwer-Visser, J., Ramirez, M. J., Kim, C. H., Hebert, T. M., Lin, J., & Horwitz, S. B. (2010). Insulin-like growth factor 2 expression modulates taxol resistance and is a candidate biomarker for reduced disease-free survival in ovarian cancer. *Clinical Cancer Research, 16*(11), 2999–3010.

Kaipio, K., Chen, P., Roering, P., Huhtinen, K., Mikkonen, P., Ostling, P., & Carpen, O. (2020). ALDH1A1-related stemness in high-grade serous ovarian cancer is a negative prognostic indicator but potentially targetable by EGFR/mTOR-PI3K/aurora kinase inhibitors. *Journal of Pathology, 250*(2), 159–169.

Kim, K., Lee, C. S., & Na, K. (2016). Light-controlled reactive oxygen species (ROS)-producible polymeric micelles with simultaneous drug-release triggering and endo/lysosomal escape. *Chemical Communications, 52*(13), 2839–2842.

Kondo, T. (2007). Stem cell-like cancer cells in cancer cell lines. *Cancer Biomarkers, 3*(4–5), 245–250.

Landen, C. N., Goodman, B., Katre, A. A., Steg, A. D., Nick, A. M., Stone, R. L., & Sood, A. K. (2010). Targeting aldehyde dehydrogenase cancer stem cells in ovarian cancer. *Molecular Cancer Therapeutics, 9*(12), 3186–3199.

Lee, J., Jenjob, R., Davaa, E., & Yang, S. G. (2019). NIR-responsive ROS generating core and ROS-triggered 5 '-Deoxy-5-fluorocytidine releasing shell structured water-swelling microgel for locoregional combination cancer therapy. *Journal of Controlled Release, 305*, 120–129.

Lee, J., Ko, S., Kwon, C. H., Lima, M. D., Baughman, R. H., & Kim, S. J. (2016). Carbon nanotube yarn-based glucose sensing artificial muscle. *Small, 12*(15), 2085–2091.

Li, X. X., Lewis, M. T., Huang, J., Gutierrez, C., Osborne, C. K., Wu, M. F., & Chang, J. C. (2008). Intrinsic resistance of tumorigenic breast cancer cells to chemotherapy. *Journal of the National Cancer Institute, 100*(9), 672–679.

Longley, D. B., & Johnston, P. G. (2005). Molecular mechanisms of drug resistance. *Journal of Pathology, 205*(2), 275–292.

Mallidi, S., Anbil, S., Bulin, A. L., Obaid, G., Ichikawa, M., & Hasan, T. (2016). Beyond the barriers of light penetration: Strategies, perspectives and possibilities for photodynamic therapy. *Theranostics, 6*(13), 2458–2487.

Martins, S., Farinha, J. P. S., Baleizao, C., & Berberan-Santos, M. N. (2014). Controlled release of singlet oxygen using diphenylanthracene functionalized polymer nanoparticles. *Chemical Communications, 50*(25), 3317–3320.

Miyazaki, O., Sekine, K., Nakajima, N., Ichimura, E., Ebara, K., Nagai, D., & Morino, T. (2014). Antimyeloma activity of NK012, a micelle-forming macromolecular prodrug of SN-38, in an orthotopic model. *International Journal of Cancer, 134*(1), 218–223.

Najafi, M., Mortezaee, K., & Majidpoor, J. (2019). Cancer stem cell (CSC) resistance drivers. *Life Sciences, 234*.

Nie, L. J., Li, F. L., Huang, X. L., Aguilar, Z. P., Wang, Y. A., Xiong, Y. H., & Xu, H. Y. (2018). Folic acid targeting for efficient isolation and detection of ovarian cancer CTCs from human whole blood based on two-step binding strategy. *ACS Applied Materials & Interfaces, 10*(16), 14055–14062.

Norton, N., Youssef, B., Hillman, D. W., Nassar, A., Geiger, X. J., Necela, B. M., & Knutson, K. L. (2020). Folate receptor alpha expression associates with improved disease-free survival in triple negative breast cancer patients. *NPJ Breast Cancer, 6*, 4.

Park, C. C., Mitsumori, M., Nixon, A., Recht, A., Connolly, J., Gelman, R., & Schnitt, S. J. (2000). Outcome at 8 years after breast-conserving surgery and radiation therapy for invasive breast cancer: Influence of margin status and systemic therapy on local recurrence. *Journal of Clinical Oncology, 18*(8), 1668–1675.

Park, C. C., Zhang, H. J., Yao, E. S., Park, C. J., & Bissell, M. J. (2008). beta(1) integrin inhibition dramatically enhances radiotherapy efficacy in human breast cancer xenografts. *Cancer Research, 68*(11), 4398–4405.

Perrone, E., Lopez, S., Zeybek, B., Bellone, S., Bonazzoli, E., Pelligra, S., & Santin, A. D. (2020). Preclinical activity of sacituzumab govitecan, an antibody-drug conjugate targeting trophoblast cell-surface antigen 2 (Trop-2) linked to the active metabolite of irinotecan (SN-38), in ovarian cancer. *Frontiers Oncology, 10*.

Ray, G. B., Chakraborty, I., & Moulik, S. P. (2006). Pyrene absorption can be a convenient method for probing critical micellar concentration (cmc) and indexing micellar polarity. *Journal of Colloid and Interface Science, 294*(1), 248–254.

Riganti, C., & Contino, M. (2019). New strategies to overcome resistance to chemotherapy and immune system in cancer. *International Journal of Molecular Sciences, 20*(19).

Rudnick, P. A., Markey, S. P., Roth, J., Mirokhin, Y., Yan, X. J., Tchekhovskoi, D. V., & Stein, S. E. (2016). A description of the clinical proteomic tumor analysis consortium (CPTAC) common data analysis pipeline. *Journal of Proteome Research, 15*(3), 1023–1032.

Sadzuka, Y., Takabe, H., & Sonobe, T. (2005). Liposomalization of SN-38 as active metabolite of CPT-11. *Journal of Controlled Release, 108*(2–3), 453–459.

Santi, D. V., Schneider, E. L., & Ashley, G. W. (2014). Macromolecular prodrug that provides the irinotecan (CPT-11) active-metabolite SN-38 with ultralong half-life, low C-max, and low glucuronide formation. *Journal of Medicinal Chemistry, 57*(6), 2303–2314.

Shibata, M., & Hoque, M. O. (2019). Targeting cancer stem cells: A strategy for effective eradication of cancer. *Cancers, 11*(5).

Swanton, C. (2012). Intratumor heterogeneity: Evolution through space and time. *Cancer Research, 72*(19), 4875–4882.

Szarynska, M., Olejniczak, A., Kobiela, J., Spychalski, P., & Kmiec, Z. (2017). Therapeutic strategies against cancer stem cells in human colorectal cancer. *Oncology Letters, 14*(6), 7653–7668.

Tahara, M., Inoue, T., Sato, F., Miyakura, Y., Horie, H., Yasuda, Y., & Sugano, K. (2014). The use of olaparib (AZD2281) potentiates SN-38 cytotoxicity in colon cancer cells by indirect inhibition of Rad51-mediated repair of DNA double-strand breaks. *Molecular Cancer Therapeutics, 13*(5), 1170–1180.

Tao, Y. F., Li, H., Huang, R. Y., Mo, D., Zeng, T., Fang, M., & Li, M. Q. (2018). Clinicopathological and prognostic significance of cancer stem cell markers in ovarian cancer patients: Evidence from 52 studies. *Cellular Physiology and Biochemistry, 46*(4), 1716–1726.

Torre, L. A., Trabert, B., DeSantis, C. E., Miller, K. D., Samimi, G., Runowicz, C. D., & Siegel, R. L. (2018). Ovarian cancer statistics, 2018. *Ca-A Cancer Journal for Clinicians, 68*(4), 284–296.

Wang, W. J., Zhang, X. Q., Li, Z. Q., Pan, D. Y., Zhu, H. Y., Gu, Z. W., & Luo, K. (2021). Dendronized hyaluronic acid-docetaxel conjugate as a stimuli-responsive nano-agent for breast cancer therapy. *Carbohydrate Polymers, 267*.

Wang, Y. Q., Yang, X., Yuan, M. Q., Xian, S., Zhang, L., Yang, D. Y., & Cheng, Y. X. (2019). Promotion of ovarian cancer cell invasion, migration and colony formation by the miR-21/Wnt/CD44v6 pathway. *Oncology Reports, 42*(1), 91–102.

Xiao, C. S., Ding, J. X., Ma, L. L., Yang, C. G., Zhuang, X. L., & Chen, X. S. (2015). Synthesis of thermal and oxidation dual responsive polymers for reactive oxygen species (ROS)-triggered drug release. *Polymer Chemistry, 6*(5), 738–747.

Xie, R., Mathijssen, R. H. J., Sparreboom, A., Verweij, J., & Karlsson, M. O. (2002). Clinical pharmacokinetics of irinotecan and its metabolites: A population analysis. *Journal of Clinical Oncology, 20*(15), 3293–3301.

Yu, S. S., Koblin, R. L., Zachman, A. L., Perrien, D. S., Hofmeister, L. H., Giorgio, T. D., & Sung, H. J. (2011). Physiologically relevant oxidative degradation of oligo(proline) cross-linked polymeric scaffolds. *Biomacromolecules, 12*(12), 4357–4366.

Zhang, H., Liu, T., Zhang, Z., Payne, S. H., Zhang, B., McDermott, J. E., & Investigators, C. (2016). Integrated proteogenomic characterization of human high-grade serous ovarian cancer. *Cell, 166*(3), 755–765.

Zhang, J. A., Xuan, T., Parmar, M., Ma, L., Ugwu, S., Ali, S., & Ahmad, I. (2004). Development and characterization of a novel liposome-based formulation of SN-38. *International Journal of Pharmaceutics, 270*(1–2), 93–107.

Zhang, S., Balch, C., Chan, M. W., Lai, H. C., Matei, D., Schilder, J. M., & Nephew, K. P. (2008). Identification and characterization of ovarian cancer-initiating cells from primary human tumors. *Cancer Research, 68*(11), 4311–4320.

Zhang, X. Q., Wu, Y. H., Li, Z. Q., Wang, W. J., Wu, Y. P., Pan, D. Y., & Luo, K. (2020). Glycodendron/pyropheophorbide-a (Ppa)-functionalized hyaluronic acid as a nanosystem for tumor photodynamic therapy. *Carbohydrate Polymers, 247*.